RESEARCH ARTICLE | NOVEMBER 04 2019

(111)-oriented, single crystal diamond tips for nanoscale scanning probe imaging of out-of-plane magnetic fields



Appl. Phys. Lett. 115, 192401 (2019) https://doi.org/10.1063/1.5127101





Articles You May Be Interested In

Scanning nitrogen-vacancy magnetometry down to 350 \mbox{mK}

Appl. Phys. Lett. (May 2022)

Scanning nitrogen-vacancy center magnetometry in large in-plane magnetic fields

Appl. Phys. Lett. (February 2022)

Magneto-optical magnetometry of individual 30 nm cobalt nanowires grown by electron beam induced deposition

Appl. Phys. Lett. (April 2012)





(111)-oriented, single crystal diamond tips for nanoscale scanning probe imaging of out-of-plane magnetic fields

Cite as: Appl. Phys. Lett. **115**, 192401 (2019); doi: 10.1063/1.5127101 Submitted: 9 September 2019 · Accepted: 22 October 2019 · Published Online: 4 November 2019







D. Rohner, J. Happacher, P. Reiser, M. A. Tschudin, A. Tallaire, J. Achard, D. B. J. Shields, and P. Maletinsky D. B. J. Shields, D. Maletinsky D. B. J. Shields, D. Shields, D. Maletinsky D. B. J. Shields, D. S

AFFILIATIONS

- Department of Physics, University of Basel, Klingelbergstrasse 82, Basel CH-4056, Switzerland
- ²LSPM-CNRS, UPR 3407, Université Paris 13, Sorbonne Paris Cité, 99 avenue Jean-Baptiste Clément, 93430 Villetaneuse, France

ABSTRACT

We present an implementation of all-diamond scanning probes for scanning nitrogen-vacancy (NV) magnetometry fabricated from (111)-oriented diamond material. The realized scanning probe tips on average contain single NV spins, a quarter of which have their spin quantization axis aligned parallel to the tip direction. Such tips enable single-axis vector magnetic field imaging with a nanoscale resolution, where the measurement axis is oriented normal to the scan plane. We discuss how these tips bring multiple practical advantages for NV magnetometry, in particular, regarding quantitative analysis of the resulting data. We further demonstrate the beneficial optical properties of NVs oriented along the tip direction, such as polarization-insensitive excitation, which simplifies optical setups needed for NV magnetometry. Our results will be impactful for scanning NV magnetometry in general and for applications in spintronics and the investigation of thin film magnets in particular.

© 2019 Author(s). All article content, except where otherwise noted, is licensed under a Creative Commons Attribution (CC BY) license (http://creativecommons.org/licenses/by/4.0/). https://doi.org/10.1063/1.5127101

Scanning probe magnetometry using nitrogen-vacancy (NV) center electronic spins in diamond offers a unique combination of spatial resolution, magnetic field sensitivity, and quantitative magnetic imaging. These combined performance characteristics have led to room-temperature imaging of single electron spins, ananoscale domains in multiferroics, and antiferromagnets, and to cryogenic experiments addressing superconductors. and magnetism in atomically thin crystals. These and other studies have demonstrated how scanning NV magnetometers can yield valuable insights into materials of high scientific and technological interest, beyond the capacity of existing nanoscale imaging methods.

Magnetometry based on NV center spins ¹⁰ builds on the extraordinary properties of this point defect in diamond that consists of a nitrogen atom adjacent to a lattice vacancy [Fig. 1(a)]. The negatively charged NV center has a ground state electronic spin-1, which is quantized along the NV binding axis, e_{NV}, and which can be readily initialized and readout by optical pumping and spin-dependent fluorescence.¹¹ These properties, along with the NV spin's response to magnetic fields through the Zeeman effect, render the NV spin an effective single-axis vector magnetometer, where, e.g., optically detected magnetic resonance (ODMR) can be employed for precise

measurements of $B_{\rm NV} = {\bf B}_{\rm ext} \cdot {\bf e}_{\rm NV}$, the projection of an external magnetic field ${\bf B}_{\rm ext}$ onto ${\bf e}_{\rm NV}$.

All-diamond scanning probes hosting individual NV spins in nanopillars [Fig. 1(b)] offer a particularly powerful approach to perform nanoscale NV magnetometry and have been the basis of key achievements in the field. All reported implementations of such scanning probes thus far consisted of diamond tips fabricated from (100)-oriented starting material—the most commonly available crystal orientation for high purity diamonds. As a result, such (100)-oriented scanning probes yield nanoscale magnetic field maps of $B_{\rm NV}$, where the measurement axis ${\bf e}_{\rm NV} \parallel \langle 111 \rangle$ is oriented at 54.7° from the sample normal. However, as will be discussed in the following, such vector magnetometry obtained with oblique measurement angles does not offer the optimal measurement configuration and could be significantly improved if NV centers oriented normal to the scanning plane could be employed.

It has been well established in scanning probe magnetic imaging that single-axis vector magnetometers measuring the out-of-plane (OOP) magnetic field component with respect to the scanning plane yield the best possible measurement configuration, ¹³ in particular, to determine quantitative information about the underlying sample

^{a)}Author to whom correspondence should be addressed: patrick.maletinsky@unibas.ch

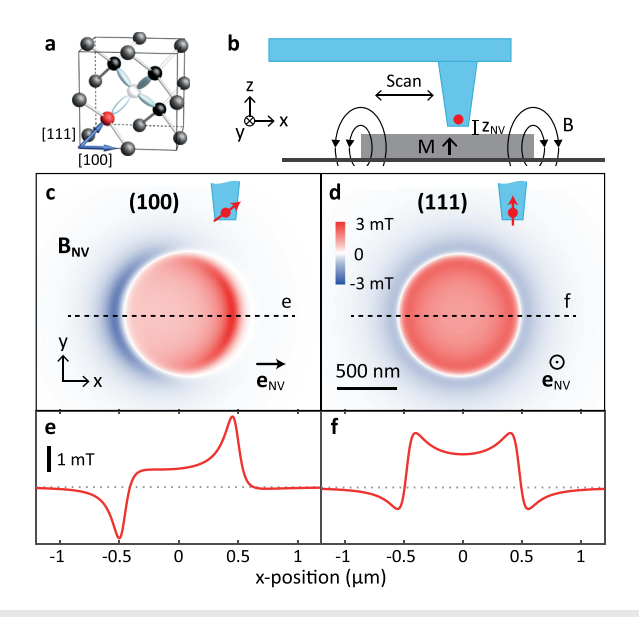


FIG. 1. (a) Atomic structure of the diamond NV center. The nitrogen atom and vacancy are represented by red and white spheres, with the [111] and [100] directions as indicated. (b) Schematic of scanning nitrogen-vacancy (NV) center magnetometry with an all-diamond probe containing a single NV center (red point). The NV is scanned at height $z_{\rm NV}$ over a thin-film magnet (where typically, $z_{\rm NV} \sim 30-80$ nm). (c) Calculated magnetic field map $B_{\rm NV}(x,y)$ for a (100)-oriented diamond tip, with $z_{\rm NV}=70$ nm, a disk diameter of 1 μ m, and an areal disk magnetization of 1 mA. (d) The same as in (c) but for an out-of-plane (OOP)-oriented NV in a (111)-oriented diamond tip. [(e) and (f)] Linecuts through the maps shown in [(c) and (d)]. Only for the OOP-oriented NV magnetometer, the rotational symmetry of the sample is retained in $B_{\rm NV}$.

magnetization.¹⁴ The key underlying reason is that a vector magnetic field image of any in-plane field component inherently lacks information about Fourier components of the magnetic field map corresponding to k-vectors perpendicular to the measurement axis. An OOP vector magnetometer is therefore the only configuration that avoids such a loss of information, yielding a better signal-to-noise ratio in commonly employed reverse propagation methods. 13,15 Additionally, stray field maps obtained using non-OOP magnetometers exhibit distortions, which complicate their direct interpretation, as illustrated by the calculated maps shown in Figs. 1(c) and 1(d). Besides these general advantages of an OOP measurement axis, the photophysics of the NV center demands that the NV axis \mathbf{e}_{NV} is aligned to the external magnetic field for field amplitudes ≥10 mT in order to maintain sizable ODMR contrasts.¹⁶ For studies of many prominent physical phenomena, such as quantum Hall¹⁷ or Skyrmion¹⁸ physics, this requirement can only be satisfied by an OOP NV orientation. Finally, an OOP NV orientation is also advantageous in that it maximizes the overlap of the NV optical dipoles with the waveguide mode of the scanning diamond nanopillar and thereby optimizes the optical addressing of NV spins. 15

Based on this general motivation, we present an experimental realization of scanning NV magnetometry tips with OOP oriented NV spins. Such devices require the use of (111)-oriented diamond for scanning probe fabrication, where one of the four possible NV orientations is aligned with the [111] axis and OOP with regard to the resulting scan plane. Fabrication of diamond nanopillars on (111)-oriented diamond has been demonstrated previously; however, no scanning

probe fabrication or NV magnetometry operation has been demonstrated for this crystal orientation thus far. In this work, we overcome this shortcoming, characterize the key properties of our resulting (111)-oriented, all-diamond scanning probes, and experimentally demonstrate their performance in nanoscale magnetic imaging.

The starting point for our fabrication was electronic grade, (111)-oriented single crystal diamond (IIa technologies), which was laser-cut and polished to a 50 μ m thin diamond plate. Near-surface NV centers were created by ion-implantation with 14 N at 6 keV and a density of 3 \times 10 11 cm $^{-2}$, followed by vacuum annealing at 800 °C. Following the fabrication recipe reported elsewhere, this implantation density resulted in an average of two NV centers per scanning probe. We obtained arrays of 10 μ m \times 20 μ m sized cantilevers holding \sim 300 nm diameter nanopillars, where cantilevers and pillars had a depth of 2 μ m each [Fig. 2(a)]. For scanning probe magnetometry, individual all-diamond cantilevers were detached from bulk diamond using micromanipulators and suitably attached to a quartz tuning fork for atomic force feedback control. 2

To characterize the resulting NV scanning probes for magnetometry, we performed confocal optical imaging [Fig. 2(b)] using a homebuilt confocal microscope operating under ambient conditions. The NV centers were addressed using a microscope objective with a numerical aperture of 0.8, excited nonresonantly with a green laser (532 nm), and the NV fluorescence was collected at wavelengths between 600 nm and 800 nm. A metal wire placed close to the focal spot of the microscope was used to apply microwave magnetic fields to drive NV spins for ODMR.

Our fabrication resulted in a few hundred scanning probes on the diamond chip, a subset of which was investigated for the present study. Applying a magnetic field along the sample normal allowed us to discriminate the OOP (i.e., [111])-oriented NVs from the non-OOP (i.e., $[1\bar{1}\bar{1}]$, $[\bar{1}\bar{1}\bar{1}]$, or $[\bar{1}\bar{1}]$)-oriented ones [Fig. 2(c)]. Specifically,

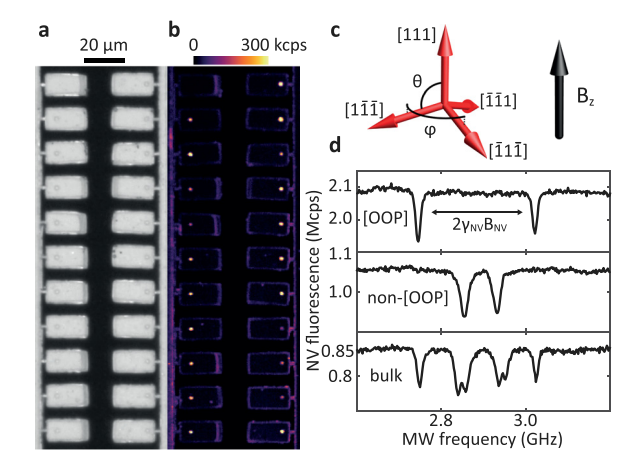


FIG. 2. (a) Optical microscopy picture of an array of finalized scanning probes fabricated from a (111)-oriented single crystal diamond. (b) The same area as in (a) imaged by confocal microscopy. Bright dots on the cantilevers correspond to nanopillars containing varying numbers of NV centers. (c) Visualization of the NV orientations and the applied magnetic field in the z-direction. φ and θ denote the angles in the spherical coordinate system. (d) ODMR spectra recorded on differently oriented NV centers in scanning probes and bulk diamond in an approximately OOP bias magnetic field of 5 mT, yielding an almost perfect overlap of the three non-OOP NV orientations.

ODMR of OOP-oriented NVs shows a Zeeman splitting $2\gamma_{\rm NV}B_{\rm NV}$, with $\gamma_{\rm NV}=28\,{\rm GHz/T}$ being the NV's gyromagnetic ratio, which is three times larger than that of the other three orientations [Fig. 2(d)].

In addition, we explored the excitation polarization dependence of NV fluorescence in our devices. This allows for a microwave-free discrimination of NV orientations, based on the fact that the NV center's optical transitions are related to two optical dipoles lying in the plane orthogonal to the NV axis. For linearly polarized excitation well below saturation, the NV excitation rate is then directly proportional to the projection of the excitation polarization onto these dipoles. Basic geometrical considerations yield the dependence of fluorescence intensity $I_{\rm NV}$ on the angle of excitation polarization φ_e as $I_{\rm NV}(\varphi_e) = I_0$ for OOP-oriented NVs and $I_{\rm NV}(\varphi_e) = I_0[\sin^2(\varphi_e - \varphi_{\rm NV})]$ otherwise, where $\varphi_{\rm NV}$ is the azimuthal angle of the NV axis [cf. Fig. 2(c)]. 21,22

In our experiment, we used a liquid crystal polarization rotator (Thorlabs) to rotate the linear polarization of the excitation laser, set to a power below NV saturation, while collecting single NV fluorescence without polarization discrimination. Figure 3(a) shows data for three representative NVs oriented along the three non-OOP-oriented NV axes, where we observe distinct minima of $I(\varphi_e)$, reaching $\sim 0.23 \, I_0$ at $\varphi_e = \varphi_{\rm NV}$ for each dataset. As expected, $\varphi_{\rm NV}$ is shifted by $\pm 120^\circ$ between the three cases. The minima of $I(\varphi_e)$ exceed the expected value of $\frac{1}{9}I_0$ —an observation we assign to background fluorescence and the onset of optical saturation. For the OOP-oriented NV centers [Fig. 3(b)], we observe a weak polarization dependence, which we attribute to mechanisms that break the cylindrical symmetry of the examined structures, such as off-center positioning of the NV centers in the pillar, $^{19.23}$ asymmetric pillar shapes, or transverse strain experienced by the NV.

Finally, we conducted experiments to demonstrate the practical benefits of OOP-oriented single NV centers by using the corresponding tip for nanoscale magnetic imaging. For this, we mapped stray magnetic fields emerging from a thin magnetic film [Ta/CoFeB (1 nm)/MgO] with OOP magnetization, as commonly employed for experiments in spintronics and skyrmionics. ^{25,26} The sample was patterned into an arrangement of 1 μ m wide stripes to generate a nontrivial stray field distribution. For magnetometry, the scanning NV center was positioned in the focus of the confocal microscope, while the

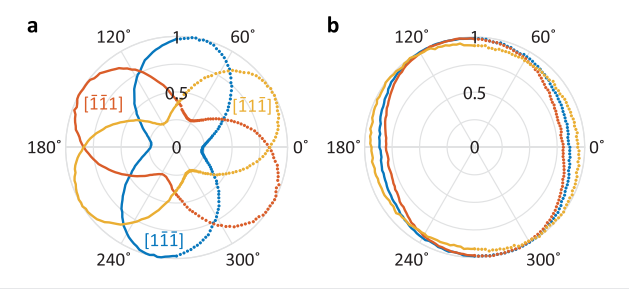


FIG. 3. (a) Dependence of NV fluorescence intensity on excitation polarization angle $\varphi_{\rm e}$ for the three NV center orientations away from the out-of-plane (OOP) direction. The strong dependence on the polarization angle allows for the determination of the NV orientation. (b) The same as in (a) for three OOP-oriented NV centers, all of which show only a weak dependence on the polarization angle. For both graphs, points show the experimentally measured data, while lines correspond to the same data shifted by 180°. For each dataset, fluorescence is normalized its maximal value.

sample was scanned laterally below the tip, with the distance between the tip and the sample stabilized by atomic force feedback.² At each point of the scan, we recorded an ODMR spectrum to determine B_{NV} .

A typical NV magnetometry image obtained over a "T-shaped" section of the CoFeB pattern is shown in Fig. 4(a). The key outcome of employing an OOP-oriented NV for this experiment is that the measured stray field shows qualitatively the same behavior at every edge of the magnetic film, irrespective of edge orientation. Specifically, $B_{\rm NV}$ shows a sharp sign-reversal with a zero-crossing and a near-perfect antisymmetric behavior along the magnetic film edge [Figs. 4(c) and 4(d)]. This behavior is in strong contrast to magnetometry with non-OOP oriented scanning NV centers, 5.6.8.9 where the qualitative behavior of $B_{\rm NV}$ near sample edges depends strongly on the orientation of the edge [Fig. 4(b)]. The quantitative data obtained with our tip can be fitted by an analytical model, from which sample magnetization M and NV-sample distance $z_{\rm NV}$ can be readily extracted. In the present case, where only the OOP component of the stray field is measured, the model for all edges takes the same and particularly simple form,

$$B_{\rm NV}(\tilde{x}) = B_z(\tilde{x}) = -\frac{\mu_0 M}{2\pi} \frac{\tilde{x}}{\tilde{x}^2 + z_{\rm NV}^2},\tag{1}$$

where \tilde{x} represents the lateral displacement from the magnet edge, μ_0 the vacuum permeability, and M the two-dimensional sample magnetization. A fit to the linecuts in Figs. 4(c) and 4(d) gave $M=1.07\pm0.02$ mA and $z_{\rm NV}=81\pm17$ nm, 78 ± 2 nm, and 55 ± 2 nm for the three edges observed. The difference in $z_{\rm NV}$ found between the

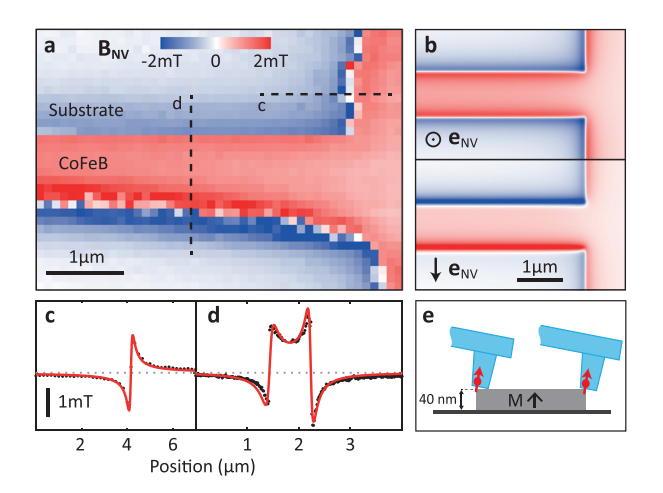


FIG. 4. (a) Two-dimensional map of $B_{\rm NV}$ obtained with an OOP-oriented NV center on a patterned, 1 nm thin CoFeB film in an OOP bias magnetic field of 4 mT. (b) Simulation of $B_{\rm NV}$ from a "T-shaped" sample as measured by an OOP NV (top) and by an NV with $\theta_{\rm NV}=54.7^\circ$ and $\varphi_{\rm NV}=-90^\circ$ (bottom), using $M=1\,{\rm mA}$ and $z_{\rm NV}=70\,{\rm nm}$. The same color scale as in (a). (c) and (d) Independently measured linecuts of $B_{\rm NV}$ along the lines indicated in (a). The red lines are analytical fits to the data (see the text), which allow for a quantitative determination of M and $z_{\rm NV}$. Importantly, and in contrast to other NV orientations, $B_{\rm NV}$ shows the same antisymmetric behavior across each sample edge, irrespective of edge orientation. (e) Illustration of the tilt-induced variation of $z_{\rm NV}$ between adjacent edges, responsible for the unequal maxima of $B_{\rm NV}$ between the three CoFeB edges observed in (c) and (d). Note that the spatial sampling rate chosen for the image in (a) slightly exacerbates this asymmetry, compared to the more highly sampled line cuts in (c) and (d).

different edges can be explained by geometrical factors originating from a small angular misalignment of the scanning tip with respect to the sample normal [Fig. 4(e)]. Importantly, we find in all cases that $z_{\rm NV}$ is clearly below 100 nm, demonstrating the excellent spatial resolution of our (111)-oriented diamond probes in NV magnetometry.

In conclusion, we have demonstrated a realization of (111)oriented diamond probes for scanning NV magnetometry, with NV spins oriented normal to the scan plane. With our experiments, including a nanoscale magnetic image using such tips, we have demonstrated how this measurement configuration brings practical advantages at various levels for NV magnetometry. Next to the general advantages for scanning magnetometry, we have also demonstrated specific advantages with respect to the probe's nanophotonic properties. The insensitivity of the NV's optical response to the orientation of linearly polarized laser excitation reduces the required optical powers and lowers experimental complexity for an optimized sensing apparatus. As was shown in earlier works, the orientation of the optical dipoles of OOP-oriented NVs is also beneficial for NV fluorescence collection efficiency and thereby for magnetometry sensitivity. 19,21 Future improvements of our (111)-oriented diamond probes will further optimize this aspect and, together with the advantages of NV magnetometry demonstrated in this paper, will be beneficial for a wide range of applications of scanning NV magnetometry in nanomagnetism and mesoscopic physics.

We thank V. Jacques, J.-V. Kim, and J. Kölbl for helpful comments and K. Garcia and R. Soucaille for fabrication of the CoFeB sample investigated. We gratefully acknowledge financial support through the NCCR QSIT (Grant No. 185902), the Basel QCQT doctoral school, through the EU Quantum Flagship project ASTERIQS (Grant No. 820394), and through the Swiss NSF Project Grants Nos. 169321 and 155845.

REFERENCES

- ¹P. Maletinsky, S. Hong, M. S. Grinolds, B. Hausmann, M. D. Lukin, R. L. Walsworth, M. Loncar, and A. Yacoby, "A robust scanning diamond sensor for nanoscale imaging with single nitrogen-vacancy centres," Nat. Nanotechnol. 7, 320 (2012).
- ²P. Appel, E. Neu, M. Ganzhorn, A. Barfuss, M. Batzer, M. Gratz, A. Tschöpe, and P. Maletinsky, "Fabrication of all diamond scanning probes for nanoscale magnetometry," Rev. Sci. Instrum. 87, 063703 (2016).
- ³M. S. Grinolds, S. Hong, P. Maletinsky, L. Luan, M. D. Lukin, R. L. Walsworth, and A. Yacoby, "Nanoscale magnetic imaging of a single electron spin under ambient conditions," Nat. Phys. 9, 215 (2013).
- ⁴I. Gross, W. Akhtar, V. Garcia, L. J. Martínez, S. Chouaieb, K. Garcia, C. Carrétéro, A. Barthélémy, P. Appel, P. Maletinsky, J.-V. Kim, J. Y. Chauleau, N. Jaouen, M. Viret, M. Bibes, S. Fusil, and V. Jacques, "Real-space imaging of non-collinear antiferromagnetic order with a single-spin magnetometer," Nature 549, 252 (2017).
- ⁵P. Appel, B. J. Shields, T. Kosub, N. Hedrich, R. Hübner, J. Faßbender, D. Makarov, and P. Maletinsky, "Nanomagnetism of magnetoelectric granular thin-film antiferromagnets," Nano Lett. 19, 1682 (2019).
- ⁶L. Thiel, D. Rohner, M. Ganzhorn, P. Appel, E. Neu, B. Müller, R. Kleiner, D. Koelle, and P. Maletinsky, "Quantitative nanoscale vortex imaging using a cryogenic quantum magnetometer," Nat. Nanotechnol. 11, 677 (2016).
- ⁷M. Pelliccione, A. Jenkins, P. Ovartchaiyapong, C. Reetz, E. Emmanouilidou, N. Ni, and A. C. Bleszynski Jayich, "Scanned probe imaging of nanoscale magnetism at cryogenic temperatures with a single-spin quantum sensor," Nat. Nanotechnol. 11, 700 (2016).

- ⁸D. Rohner, L. Thiel, B. Müller, M. Kasperczyk, R. Kleiner, D. Koelle, and P. Maletinsky, "Real-space probing of the local magnetic response of thin-film superconductors using single spin magnetometry," Sensors 18, 3790 (2018).
- ⁹L. Thiel, Z. Wang, M. A. Tschudin, D. Rohner, I. Gutiérrez-Lezama, N. Ubrig, M. Gibertini, E. Giannini, A. F. Morpurgo, and P. Maletinsky, "Probing magnetism in 2D materials at the nanoscale with single-spin microscopy," Science 364, 973–976 (2019).
- ¹⁰L. Rondin, J.-P. Tetienne, T. Hingant, J.-F. Roch, P. Maletinsky, and V. Jacques, "Magnetometry with nitrogen-vacancy defects in diamond," Rep. Prog. Phys. 77, 56503 (2014).
- ¹¹A. Gruber, A. Drabenstedt, C. Tietz, L. Fleury, J. Wrachtrup, and C. Borczyskowski, "Scanning confocal optical microscopy and magnetic resonance on single defect centers," Science 276, 2012 (1997).
- ¹²P. Appel, M. Ganzhorn, E. Neu, and P. Maletinsky, "Nanoscale microwave imaging with a single electron spin in diamond," New J. Phys. 17, 112001 (2015).
- 13E. A. Lima and B. P. Weiss, "Obtaining vector magnetic field maps from single-component measurements of geological samples," J. Geophys. Res. 114, B06102, https://doi.org/10.1029/2008/B006006 (2009).
- ¹⁴F. Casola, T. van der Sar, and A. Yacoby, "Probing condensed matter physics with magnetometry based on nitrogen-vacancy centres in diamond," Nat. Rev. Mater. 3, 17088 (2018).
- ¹⁵B. J. Roth, N. G. Sepulveda, and J. P. Wikswo, "Using a magnetometer to image a two-dimensional current distribution," J. Appl. Phys. 65, 361 (1989).
- 16J.-P. Tetienne, L. Rondin, P. Spinicelli, M. Chipaux, T. Debuisschert, J.-F. Roch, and V. Jacques, "Magnetic-field-dependent photodynamics of single NV defects in diamond: An application to qualitative all-optical magnetic imaging," New J. Phys. 14, 103033 (2012).
- 17Y. Zhang, Y.-W. Tan, H. L. Stormer, and P. Kim, "Experimental observation of the quantum Hall effect and Berry's phase in graphene," Nature 438, 201 (2005).
- ¹⁸N. Nagaosa and Y. Tokura, "Topological properties and dynamics of magnetic skyrmions," Nat. Nanotechnol. 8, 899 (2013).
- ¹⁹E. Neu, P. Appel, M. Ganzhorn, J. Miguel-Sánchez, M. Lesik, V. Mille, V. Jacques, A. Tallaire, J. Achard, and P. Maletinsky, "Photonic nano-structures on (111)-oriented diamond," Appl. Phys. Lett. 104, 153108 (2014).
- ²⁰ J. R. Maze, A. Gali, E. Togan, Y. Chu, A. Trifonov, E. Kaxiras, and M. D. Lukin, "Properties of nitrogen-vacancy centers in diamond: The group theoretic approach," New J. Phys. 13, 025025 (2011).
- ²¹T. P. Mayer Alegre, C. Santori, G. Medeiros-Ribeiro, and R. G. Beausoleil, "Polarization-selective excitation of nitrogen vacancy centers in diamond," Phys. Rev. B 76, 165205 (2007).
- ²²M. Lesik, J.-P. Tetienne, A. Tallaire, J. Achard, V. Mille, A. Gicquel, J.-F. Roch, and V. Jacques, "Perfect preferential orientation of nitrogen-vacancy defects in a synthetic diamond sample," Appl. Phys. Lett. 104, 113107 (2014).
- ²³J. Bleuse, J. Claudon, M. Creasey, N. S. Malik, J.-M. Gérard, I. Maksymov, J.-P. Hugonin, and P. Lalanne, "Inhibition, enhancement, and control of spontaneous emission in photonic nanowires," Phys. Rev. Lett. 106, 103601 (2011).
- ²⁴A. Barfuss, M. Kasperczyk, J. Kölbl, and P. Maletinsky, "Spin-stress and spin-strain coupling in diamond-based hybrid spin oscillator systems," Phys. Rev. B 99, 174102 (2019).
- 25 J.-P. Tetienne, T. Hingant, J.-V. Kim, L. H. Diez, J.-P. Adam, K. Garcia, J.-F. Roch, S. Rohart, A. Thiaville, D. Ravelosona, and V. Jacques, "Nanoscale imaging and control of domain-wall hopping with a nitrogen-vacancy center microscope," Science 344, 1366 (2014).
- ²⁶J.-P. Tetienne, T. Hingant, L. J. Martínez, S. Rohart, A. Thiaville, L. Herrera Diez, K. Garcia, J.-P. Adam, J.-V. Kim, J.-F. Roch, I. M. Miron, G. Gaudin, L. Vila, B. Ocker, D. Ravelosona, and V. Jacques, "The nature of domain walls in ultrathin ferromagnets revealed by scanning nanomagnetometry," Nat. Commun. 6, 6733 (2015).
- 27T. Hingant, J.-P. Tetienne, L. J. Martínez, K. Garcia, D. Ravelosona, J.-F. Roch, and V. Jacques, "Measuring the magnetic moment density in patterned ultrathin ferromagnets with submicrometer resolution," Phys. Rev. Appl. 4, 014003 (2015).